# Three-Dimensional Evolution of a Relativistic Current Sheet: Triggering of Magnetic Reconnection by the Guide Field

S. Zenitani* and M. Hoshino

*Department of Earth and Planetary Science, University of Tokyo, 7-3-1, Hongo, Bunkyo, Tokyo, 113-0033 Japan*

(Received 9 April 2005; published 23 August 2005)

The linear and nonlinear evolution of a relativistic current sheet of pair ($e^{\pm}$) plasmas is investigated by three-dimensional particle-in-cell simulations. In a Harris configuration, it is obtained that the magnetic energy is fast dissipated by the relativistic drift kink instability (RDKI). However, when a current-aligned magnetic field (the so-called "guide field") is introduced, the RDKI is stabilized by the magnetic tension force and it separates into two obliquely propagating modes, which we call the relativistic drift-kink-tearing instability. These two waves deform the current sheet so that they trigger relativistic magnetic reconnection at a crossover thinning point. Since relativistic reconnection produces a lot of nonthermal particles, the guide field is of critical importance to study the energetics of a relativistic current sheet.

DOI: 10.1103/PhysRevLett.95.095001 PACS numbers: 52.27.Ep, 52.27.Ny, 52.65.Rr, 95.30.Qd

It is widely believed that plasma heating and particle acceleration occur in a wide variety of plasma regions that contain magnetic fields. A current sheet structure where the magnetic field polarity changes its direction is one of the most fundamental structures among them. Importantly, when two groups of magnetic field lines with opposite polarities meet each other around the current sheet, magnetic reconnection takes place and then it explosively dissipates the magnetic energy into the kinetic energy of plasmas. In fact, reconnection is accepted as a main player in stellar and solar flares [1] and storms in the Earth's magnetosphere [2]. The theory of reconnection has often been studied in a current sheet with antiparallel field lines, but it is possible that field lines are somehow "twisted" and so the system, with a finite amplitude of a current-aligned magnetic field (the so-called guide field), has recently been investigated by three-dimensional (3D) simulations [3–7]. Magnetic reconnection processes are also important in high-energy astrophysical contexts; the jets from active galactic nuclei [8–10], pulsar winds [11,12], and probably gamma-ray bursts [13,14]. Particularly in the Crab Nebula, it has been a long-standing problem (the so-called "$\sigma$ problem"), how originally Poynting-dominated plasmas [15] are converted into kinetic-dominated plasmas [16] in the relativistic outflow from the neutron star. The most promising solution is relativistic magnetic reconnection [17] in the striped current sheets [11].

However, reconnection processes in such relativistic hot $e^{\pm}$ plasmas (the plasma temperature $T$ is larger than the rest mass energy: $T \gg mc^2$) has been poorly understood. Recently, 2D particle simulations of relativistic magnetic reconnection in such a relativistic current sheet (RCS) were carried out [18,19]. One important point is that a lot of magnetic energy can be converted into nonthermal energy of plasmas due to the enhanced dc acceleration around the $X$-type region. By the way, a RCS is extremely unstable to the relativistic drift kink instability (RDKI) [20], a relativistic extension of the drift kink instability [21–23], whose wave vector is normal to the 2D reconnection plane. Contrary to the relativistic reconnection, the RDKI mainly dissipates magnetic energy into plasma heat rather than nonthermal energy. In addition, the effect of the guide field in a RCS has never been investigated in two and three dimensions.

We have performed 3D particle-in-cell simulations to explore linear/nonlinear evolution of a RCS, firstly taking into account the guide field effect. The system consists of $256^3$ grids. We set periodic boundaries in the $x$, $y$, and $z$ directions. In the $z$ direction, double current sheets are considered. The half-width of the current sheet $\lambda$ is set to 10 grids so that the boundaries are located at $x = \pm 12.8$, $y = \pm 12.8$, and $z = \pm 6.4$ in unit of $\lambda$. Also, time is normalized by the light transit time $\tau_c = \lambda/c$. We take a relativistic Harris model as the initial current sheet configuration [12]. The magnetic field and their distribution functions are described by $B_x = B_0 \tanh(z)$, $B_y = \alpha B_0$, $f_{\pm} \propto n(z) \exp[-\Gamma_{\beta}\{\varepsilon - \beta_{\pm} mcu_y\}/T] + n_{bg} \exp(-\varepsilon/0.1T)$, and $n(z) = n_0 \cosh^{-2}(z)$, where $B_0$ is the magnitude of the antiparallel component of the magnetic field in the lobe (the background region), $\alpha$ is the relative amplitude of the guide field to the reversed field, $n_0$ is the number density of plasmas in the current sheet, $n_{bg}$ is the number density of plasmas in the lobe, $\beta_{\pm} = v_{\pm}/c$ are the drift velocities for each species; $\beta_+ = +\beta$ for positrons, $\beta_- = -\beta$ for electrons, $\Gamma_{\beta} = [1 - \beta^2]^{-1/2}$, $\varepsilon$ is the particle energy, and $\boldsymbol{u}$ is the four velocity of $\boldsymbol{u} = [1 - (v/c)^2]^{-1/2} \boldsymbol{v}$. We investigate two cases of $\alpha = 0$ (run A) and $\alpha = -0.5$ (run B). We set $T = mc^2$ and $\beta = 0.3$. The total number of super particles is $5 \times 10^8$ and we set the plasma density to $n_0 \sim 80$ (pairs) and $n_{bg} \sim 4$ (pairs) per one grid so that $n_{bg}/n_0 = 0.05$. The total energy is conserved within an error of 0.5% throughout the simulation runs.

First, we present a result of run A without the guide field. A snapshot at $t = 80$ is presented in panel (a) in Fig. 1. The system evolution is similar to that of the 2D RDKI [20], including profiles of perturbed physical properties. The wave number of the most dominant mode is $k_y \sim 0.74$

 

(mode 3) and its growth rare is $\omega_i/\Omega_c = 0.02$, where $\Omega_c$ is the gyrofrequency; $\Omega_c = \omega_c/\gamma = (eB_0)/(\gamma mc)$, $\gamma$ is the Lorenz factor for typical particle energy. In the 2D work, the growth rate has its peak around $k_y \sim 0.7$–$0.8$ at $\omega_i/\Omega_c = 0.03$–$0.04$. After this stage, the RCS becomes folded, turns into the nonlinear stage, and then mixed into the turbulent state. Because of the limited simulation height in $z$, some plasmas are also mixed across the $z$ boundaries. Finally, more than 83% of the magnetic energy is dissipated into the particle energy. Figure 2 shows energy spectra of 3D runs. For run A, three stages ($t = 0, 80, 140$) are presented. In the later time of $t = 140$, one can recognize a high-energy tail due to the particle acceleration inside the folded current sheet. More importantly, plasmas are heated throughout the late-time mixing stage of the RDKI. The transportation across the $z$ boundaries provides no significant change between two dimensions and three dimensions in the spectra. We think that the observed growth rate becomes slower than that of two dimensions due to the limited system size in $z$. Note that it is still faster than that of 2D reconnection ($\omega_i/\Omega_c = 0.011$). Since the RDKI grows faster when $T \gtrsim mc^2$ [20], we conclude that the RDKI is a dominant process in a RCS. Again, magnetic dissipation and plasma heating by the RDKI would be the main signature of a RCS.

Next, we show results of run B with a finite amplitude of the guide field $B_y = -0.5B_0$. Snapshots at two stages ($t = 120$ and 170) are presented in panels (b), (c) and (d) in Fig. 1. Instead of the RDKI, a flutelike mode whose wave vector is $\boldsymbol{k}_1 = (0.25, 0.25)$, is observed on the upper side of the RCS at $t = 120$ in Fig. 1(b). A similar flute mode is observed on the lower side, too, but its wave vector is in a different direction: $\boldsymbol{k}_2 = (0.25, -0.25)$. In order to take a clear look at this lower side mode, we present cross sections at $z = -1$ in panels (b) and (c). Snapshots at $t = 170$ are presented in panels (c) and (d) in Fig. 1. Because of the two flute modes, the RCS is so modulated that a plasma density hole appears at the center. In panel (d), cross sections of the RCS at $x, y, z = 0$, and typical magnetic field lines are presented. Magnetic reconnection occurs around the center of the simulation box. The speed of reconnection jets is up to $0.6c$ and the outflow plasmas are transported into the $O$ point(s) around $(x, y) \sim (\pm 12.8, 0)$. Then, since the magnetic field mainly consists of the guide

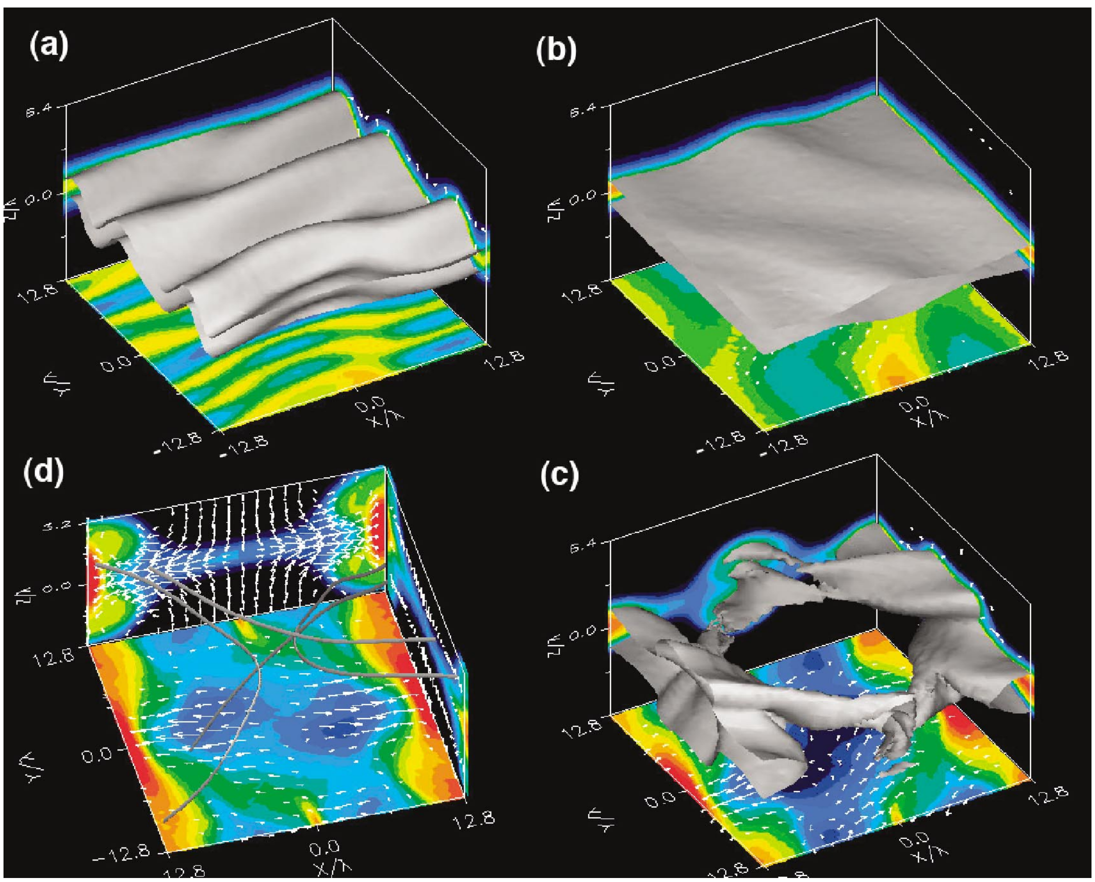


FIG. 1 (color). (a) Snapshot of the current sheet in run A ($\alpha = 0$) at $t = 80$. Two gray surfaces show $n = 2/3n_0$. The plasma density at the neutral plane ($z = 0$) is projected into the bottom roof, with color from blue (empty) to red (dense; $n \sim 1.2n_0$). The white arrows show plasma flow. The light speed ($v = c$) is projected to the length of 4. (b) Snapshot of the current sheet in run B with a guide field configuration ($\alpha = -0.5$) at $t = 120$. Two gray surfaces show $n = 2/3n_0$ and the plasma density under the neutral plane ($z = -1$) is presented in color in the bottom roof. (c) Snapshot at $t = 170$ in run B. (d) Another snapshot at $t = 170$ in run B, with typical magnetic field lines. Three projections show cross sections at $x, y, z = 0$.

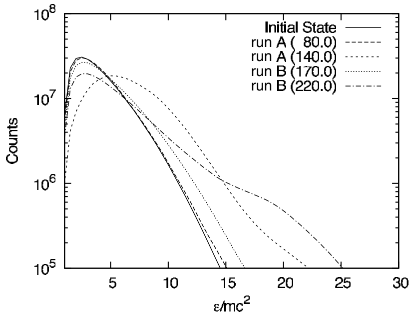


FIG. 2. Energy spectra observed in runs A and B. The initial state (the same in both two runs) and two typical stages for each run are selected. Time is normalized by $\tau_c$ and particle energy is normalized by $mc^2$.

field component $B_y$ inside the RCS, they are dissipated along the $O$-line region around $x = \pm 12.8$. The dense region around $(x, y) \sim (0, \pm 12.8)$ is the remnant of the thick point of the RCS, where two obliquely propagating modes are linked. Energy spectra in run B are also presented in Fig. 2. The oblique mode itself has few effects on the spectra, however, after relativistic reconnection starts, strong enhancement of the nonthermal tail is observed due to the particle acceleration around the $X$-type region [18,19].

Along with 3D work, we have studied an effect of the guide field using several sets of 2D particle simulations ($|\alpha| = 0, 0.25, 0.5, 1.0$). It is obtained that reconnection in the $xz$ plane grows slower when larger $|\alpha|$ is set, while we were unable to observe the RDKI in the $yz$ plane when $|\alpha|$ exceeds some critical value ($|\alpha| \gtrsim 0.5$). We found that this is due to the magnetic tension effect. When $\alpha = 0$, magnetic field lines are always parallel to the wave fronts of the instability and so they cannot be bent (no tension force), but when the guide field is introduced, the RDKI will be opposed by the tension force of current-aligned field lines.

In order to study the obliquely propagating modes in run B, we investigate eigenfunctions and their linear growth rates of instabilities in the RCS. The relativistic two-fluid equations are linearized, assuming that perturbations are given by $\delta f \propto f(z) \exp(ik_x x + ik_y y - i\omega t)$. The obtained growth rates ($\omega_i/\Omega_c$) are presented in contour maps in Fig. 3 for two cases of $\alpha = 0, -0.5$. In these maps,

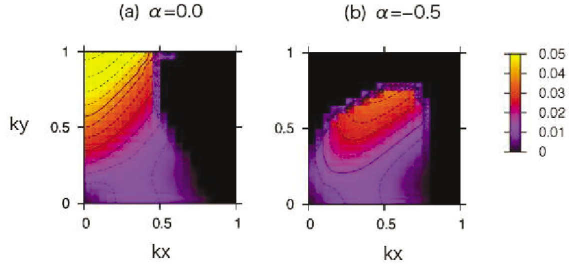


FIG. 3 (color online). Growth rate ($\omega_i/\Omega_c$) of the instabilities in wave-vector spaces of ($0 \le k_x \le 1, 0 \le k_y \le 1$). (a) $\alpha = 0$ and (b) $\alpha = -0.5$.

reconnection (tearing mode) is plotted along the $k_x$ axis and the RDKI is plotted along the $k_y$ axis. We mention that all of the obtained modes are purely growing and that growth rates for $(k_x, k_y)$ are equal to the rates for $(|k_x|, |k_y|)$ because of the symmetry. In Fig. 3(a), the RDKI or its neighbor of the relativistic drift sausage instability (RDSI) has the maximum growth rate in $k_x = 0$ while we obtain the dominant mode at $(k_x, k_y) \sim (0, 0.74)$ in the 3D simulation. We note that these instabilities are dumped by the kinetic effect in shorter wavelengths of $|k| \gtrsim 1$, where the fluid theory is not valid. Because of the similarity of the eigenprofiles and growth rates, it is natural to say that the oblique modes are the intermediate modes between the RDKI/RDSI and the tearing instability. Hereafter we shall call them the "relativistic drift-kink-tearing instability" (RDKTI), the oblique extension of the RDKI/RDSI driven by $\boldsymbol{k}$-aligned component of the current. Since the RDKTI mode is weakly stabilized by the field lines and since its driving force is weaker, the RDKTI grows slower than relevant RDKI/RDSI in a RCS with exact antiparallel fields. When we set larger $|\alpha|$, the RDKI/RDSI along the $k_y$ axis become slower due to the magnetic tension of stronger guide field. Instead, two branches of the RDKTI for $\boldsymbol{k} = (k_x, \pm k_y)$ become dominant, or, in other words, the RDKI/RDSI separates into two branches of oblique RDKTI waves. Figure 3(b) shows the growth rate in the case of $\alpha = -0.5$. As obtained by supplemental 2D runs, the RDKI along the $k_y$ axis is stabilized by the magnetic tension. The right panel in Fig. 4 shows eigenprofiles of density perturbation for $\boldsymbol{k} = (0.25, \pm 0.25)$. They are highly asymmetric in $z$; a mode for $\boldsymbol{k}_1 = (0.25, 0.25)$ has its peak in the upper side of the RCS, while the other one for $\boldsymbol{k}_2 = (0.25, -0.25)$ has its peak in the lower side. Such asymmetry is explained by the twisted effect of background magnetic fields. In case of the mode for $\boldsymbol{k}_1$, the magnetic field is quasiperpendicular to $\boldsymbol{k}_1$ in the upper side of the RCS so that its tension can be neglected.

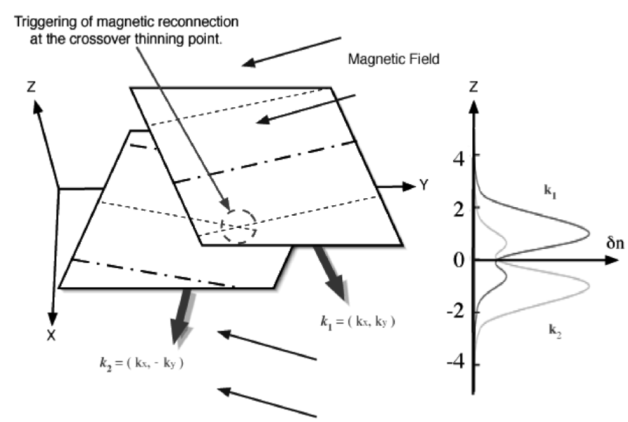


FIG. 4. Left: A schematic illustration of obliquely propagating modes and the triggering mechanism of magnetic reconnection. Right: eigenprofiles of the relativistic drift-kink-tearing modes. A gray line stands for $\boldsymbol{k}_1 = (0.25, 0.25)$ and a light gray line shows its partner: $\boldsymbol{k}_2 = (0.25, -0.25)$.

On the contrary, the field is quasiparallel to $\boldsymbol{k}_1$ in the lower side, so that the mode is opposed by strong magnetic tension. The RDKTI for $\boldsymbol{k}_2$ is an upside-down mirror of the RDKTI for $\boldsymbol{k}_1$ because of the physical symmetry. As a result, we observe two dominant RDKTI modes: one for $\boldsymbol{k}_1$ in the upper side and the other for $\boldsymbol{k}_2$ in the lower side of the RCS. As larger $|\alpha|$ is set, an angle between two oblique wave vectors (such as $\boldsymbol{k}_1$ and $\boldsymbol{k}_2$) becomes wider in accordance with the lobe magnetic field lines. In such cases, the RDKTI grows slower because of stronger magnetic tension.

The secondary relativistic reconnection is triggered by the RDKTI in its nonlinear stage. Since two major RDKTI modes are in different directions, the deformed RCS become very thin at the crossover point where both the upper and the lower RDKTI wave press the RCS. This mechanism is illustrated in Fig. 4. In addition to this enhanced thinning effect, accompanying electric fields $E_y$ and the heated plasma due to the RDKTI leads to the triggering of magnetic reconnection. Once reconnection broke up, it continued to grow and then particle acceleration took place near the reconnecting region. It produces more nonthermal particles due to the direct particle acceleration in the reconnection region [18,19]. Actually there are two crossover thinning points—one is around $(x, y) \sim (0, 0)$ and the other is around $(x, y) \sim (\pm 12.8, \pm 12.8)$. However, reconnection jets from the former point are finally transported into the latter point so that the reconnection does not dominate at the latter point. The speed of the reconnection jets is finally up to $0.78c$ at a later stage.

The electromagnetic energy ($E_{EM}$) is dissipated by the rate of $\frac{d}{dt} E_{EM} \sim -4 v_t L_x L_y B_0^2 / 8\pi$, where $L_{x,y}$ are the system size and $v_t$ is a typical dissipation speed [12,13]. We obtain $v_t \sim 0.25c$ in run A and this value is consistent with the $z$-displacement speed of the RDKI: $v_z = 0.2$–$0.3c$ [20]. In run B, $v_t \sim 0.05c$ or larger. The ratio of the total field energy ($E_{EM}$) to the total particle energy ($E_P = \Sigma \gamma mc^2$) is originally 1.0 but it falls below 0.1 at $t = 160$ in run A, while the ratio evolves from 1.25 to 0.7 at $t = 220$ in run B. Although this ratio extremely depends on the system size, it seems that the RDKI is favorable to produce kinetic-dominated plasmas.

Finally, we discuss our system size limitations. The most dominant RDKI has mode $(1, \pm 1)$ in run B. Since smaller-wavelength modes will be suppressed by the kinetic effect and since longer-wavelength RDKTI modes have smaller growth rates in Fig. 3(b), the obtained modes would be roughly correct and the trigger mechanism of reconnection should be the same as long as a pair of the RDKTI modes dominate. The global evolution of the RCS still remains unclear. One possibility is that multiple reconnection regions evolve into one big reconnection region, and then higher energetic particles will be produced in the wider acceleration region. Another possibility is that many reconnection regions grow and that the system becomes turbulent, which may contribute to statistical acceleration or thermalization. It should be further investigated by larger particle simulations or two-fluid relativistic MHD simulations.

Let us summarize this Letter. Considering the effect of the guide field, we present the following two scenarios in a RCS. One is plasma heating by the RDKI in an antiparallel case without the guide field. The other is nonthermal acceleration by secondary reconnection in a twisted case with the guide field. In this case, magnetic reconnection is triggered by the coupling of two RDKTI waves, which is separated from the RDKI/RDSI. It should be noted that slight differences in magnetic field topology have great influence on the destination of the magnetic energy: plasma thermal energy or nonthermal energy.

The authors are grateful to Dr. T. Yokoyama and Dr. A. Miura for fruitful discussions. This work was supported by the facilitates of JAXA and the Solar-Terrestrial Environment Laboratory, Nagoya University.

*Electronic address: zenitani@eps.s.u-tokyo.ac.jp

[1] E. N. Parker, J. Geophys. Res. **62**, 509 (1957).
[2] J. W. Dungey, Phys. Rev. Lett. **6**, 47 (1961).
[3] J. F. Drake, M. Swisdak, C. Cattell, M. A. Shay, B. N. Rogers, and A. Zeiler, Science **299**, 873 (2003).
[4] P. Ricci, G. Lapenta, and J. U. Brackbill, Phys. Plasmas **10**, 3554 (2003).
[5] I. Silin and J. Büchner, Phys. Plasmas **10**, 3561 (2003).
[6] P. L. Pritchett and F. V. Coroniti, J. Geophys. Res. **109**, A01 220 (2004).
[7] K. G. Tanaka, I. Shinohara, and M. Fujimoto, Geophys. Res. Lett. **31**, L22 806 (2004).
[8] T. Di Matteo, Mon. Not. R. Astron. Soc. **299**, L15 (1998).
[9] H. Lesch and G. T. Birk, Astrophys. J. **499**, 167 (1998).
[10] D. A. Larrabee, R. V. E. Lovelace, and M. M. Romanova, Astrophys. J. **586**, 72 (2003).
[11] F. V. Coroniti, Astrophys. J. **349**, 538 (1990).
[12] J. G. Kirk and O. Skjæraasen, Astrophys. J. **591**, 366 (2003).
[13] G. Drenkhahn, Astron. Astrophys. **387**, 714 (2002).
[14] G. Drenkhahn and H. C. Spruit, Astron. Astrophys. **391**, 1141 (2002).
[15] J. Arons, Space Sci. Rev. **24**, 437 (1979).
[16] C. F. Kennel and F. V. Coroniti, Astrophys. J. **283**, 694 (1984).
[17] E. G. Blackman and G. B. Field, Phys. Rev. Lett. **72**, 494 (1994).
[18] S. Zenitani and M. Hoshino, Astrophys. J. **562**, L63 (2001).
[19] C. H. Jaroschek, R. A. Treumann, H. Lesch, and M. Scholer, Phys. Plasmas **11**, 1151 (2004).
[20] S. Zenitani and M. Hoshino, Astrophys. J. **618**, L111 (2005).
[21] Z. Zhu and R. M. Winglee, J. Geophys. Res. **101**, 4885 (1996).
[22] P. L. Pritchett, F. V. Coroniti, and V. K. Decyk, J. Geophys. Res. **101**, 27 413 (1996).
[23] W. Daughton, J. Geophys. Res. **103**, 29 429 (1998).